



Traveling-Wave Micropumps

Guohua Liu and Wei Zhang

Contents

Introduction	1018
Principle	1019
Structure and Fabrication	1023
Piezoelectric Travelling-Wave Micropump	1023
Magnetic Travelling-Wave Micropump	1026
Performance	1028
Piezoelectric Travelling-Wave Micropump with Different Channels	1029
Magnetic Travelling-Wave Micropump with Different Parameters	1031
Conclusion	1034
References	1035

Abstract

In this chapter, a valveless piezoelectric and magnetic micropump driven by travelling wave is presented. The micropump, fabricated with polydimethylsiloxane (PDMS) and polymethylmethacrylate (PMMA), consists primarily of a saw-tooth microchannel, substrates, and two kinds of integrated actuator arrays (piezoelectric bimorph arrays and NdFeB permanent magnetic arrays). The travelling wave beneath the top wall of the elastic microchannel can be induced by the actuator arrays, and the liquid particles are then transported along with the travelling wave in the microchannel. The micropumps are designed and fabricated with different microchannels (the saw-tooth and the straight microchannels). Appropriate geometry of the saw-toothed micro-

G. Liu (✉) · W. Zhang

Key Laboratory of Photo-electronic Thin Film Devices and Technology of Tianjin, College of Electronic Information and Optical Engineering, Nankai University, Tianjin, China
e-mail: liugh@nankai.edu.cn

© Springer Nature Singapore Pte Ltd. 2018

Q.-A. Huang (ed.), *Micro Electro Mechanical Systems*, Micro/Nano Technologies,
https://doi.org/10.1007/978-981-10-5945-2_29

1017

channel was also studied for optimizing the performance of the micropump. Experimental characterization of the micropump has been performed in terms of the frequency response of the flow rate and back pressure. The results demonstrate that this micropump is capable of generating a stable flow rate in microfluidic systems.

Keywords

Micropumps · Travelling wave · Piezoelectric actuator arrays · Magnetic actuator arrays · Microfluidics · MEMS · PDMS microchannel

Introduction

Micropumps play an essential role in transporting precise volumes of sample fluid through the various components of microelectromechanical systems (MEMS), particularly in the fields of medical implants, drug delivery systems, lab-on-a-chip (LOC) systems, and micro-total analysis systems (μ TAS) (Wang et al. 2013; Iverson and Garimella 2008). Different driving modes are used to build the micropump such as piezoelectric, electrostatic, pneumatic, and thermodynamic. Generally, micropumps can be divided into two different types: mechanical and nonmechanical micropumps (Jang and Lee 2000; Zengerle 1995). Nonmechanical pumps usually employ the properties of the working liquid to generate the flow (Darabi et al. 2001). Therefore, the available liquids are limited and are often incompatible with biochemical protocols. On the other hand, mechanical micropumps can transport a variety of liquids and be less sensitive to liquid properties. They usually use moving parts, such as check valves, oscillating diaphragms, turbines, and gears, to deliver a constant fluid volume, which could provide a more versatile pumping solution (Muralt 2005). One type of mechanical micropump is the valveless micropump which has several advantages over other micropumps, such as no moving parts, extended working range, ease of fabrication, and cost effectiveness.

The most typical valveless micropump is the valveless nozzle/diffuser micropump which makes fluid flow by implementing diffuser and nozzle elements to function as passive check valves (Olsson et al. 1996, 1997, 2000). In nozzle/diffuser valveless micropumps, the flow field is generated typically by piezoelectric actuators which are equipped with a pressure chamber for generating a pressure difference between the inlet and outlet. Though piezoelectric micropumps can transport liquid at a high flow rate and with excellent controllability, further miniaturization is difficult because it reduces the generated pressure and because of the difficulty in fabricating a micropressure chamber using conventional MEMS processes. To solve these problems, the valveless piezoelectric travelling-wave micropump has been proposed (Ogawa et al. 2009; Zhang et al. 2011), which is advantageous for miniaturization because of its simple structure. The vibrating wall is a unimorph structure of piezoelectric thin films directly deposited on the ceiling of the microchannel. Additionally, there is no need to prepare a pressure chamber with this configuration. The principle of the piezoelectric travelling-wave micropump is that

the piezoelectric actuator array induces a travelling wave propagated outside the top wall of the microchannel, which makes the fluid particles move forward continuously. Though piezoelectric actuators usually produce high actuation forces and fast mechanical responses, they need high input voltages. Also, most piezoelectric actuators are realized by mounting standard metal-piezo-composites as membrane actuators on top of a plastic microchannel. This requires a reliable mounting and sealing technology, with the danger of wearing at the matching points of metal and polymer. Overall, the two main demerits associated with current piezoelectric travelling micropumps are (1) fabrication complexity and (2) power consumption.

In an attempt to simplify the fabrication process and to address the above demerits, a novel valveless magnetic travelling-wave micropump is presented, whose principle is that a travelling wave beneath the top wall of the elastic microchannel is generated by the interactive forces between two integrated magnetic arrays. As compared to piezoelectric types, it also has the merits of fast response time and high actuation forces but can be manufactured more easily and actuated with a relatively low voltage. In this pump, a modified nozzle/diffuser channel structure called a saw-toothed microchannel is adopted, based on the flow-resistance coefficient equations. Since previous numerical and experimental studies have demonstrated that the geometric design of the nozzle/diffuser elements can significantly affect the performance of the valveless micropump (Ye et al. 2014), systematic characterization of the microchannel has been performed. In addition, a fully printed circuit board (PCB) fabrication technology is presented in our work and the substrate used in this technology is polymethylmethacrylate (PMMA), which allows for easy fabrication and integration with other microfluidic components.

Principle

The travelling-wave micropump is similar to the peristaltic micropump in structure, but they have different working principle and different properties yet. The peristaltic micropump pumps the fluid by alternately extruding and releasing the elastic channel of the pump. As the extrusion position on the elastic channel moves alternately, negative pressure is formed in the tube, and the liquid flows along with the extrusion position movement. The flow rate of the peristaltic micropump depends on the driving frequency and force of the extrusion, and the relationship between the flow rate and driving frequency shows a linear relationship. However, the peristaltic micropump produces an unsteady pulse flow at the outlet during working. On the other hand, travelling-wave micropump depends on the travelling wave propagating along a certain direction in the elastic channel. Because of the viscosity of the fluid, the fluid in the channel moves slightly along the travelling wave propagating direction after each period and obtains a continuous directional flow rate at the outlet of the micropumps. The travelling wave in the elastic channel is excited by several standing waves at a certain vibration frequency, thus the flow rate of travelling-wave micropump is not linear with the driving frequency, which reaches the maximum at a certain frequency, and declines at both sides of the maximum. In the travelling-wave

micropumps, the fluid transport is driven by a high frequency and low amplitude travelling wave, so the flow rate of the travelling-wave micropump is relatively stable. The travelling wave in the elastic channel is generated by several standing waves, and the relationship of travelling wave and standing wave is introduced follows.

Standing waves and travelling waves have many different characteristics in physical properties, but there is a close relationship between these two waves. A travelling wave is the wave of the spatial distribution of a physical quantity that propagates forward in space and time. With difference from the travelling wave, the standing wave does not propagate forward like a travelling wave, in which each point on the axis of the wave has an associated constant amplitude. In the process of vibration, the locations at which the amplitudes is always minimum are called the wave nodes, and the locations where the amplitude can reach maximum are called the antinodes, there is always 1/4 wavelength length difference between the adjacent wave nodes and antinodes. With certain conditions, the travelling wave and standing wave can be transformed into each other. For example, the superposition of two travelling waves, which have the same amplitude, frequency, direction of vibration, and the opposite propagation direction at the same time, could obtain a travelling wave with the same frequency of two standing waves.

Standing waves do not transfer the energy in space; it means the average energy density of the standing wave is equal to zero in one period. The standing wave can be expressed as:

$$\xi(x, t) = A \cos \frac{2\pi}{\lambda} x \cdot \cos \omega t \quad (1)$$

Different from the standing wave, the travelling wave propagates continuously in the medium. Each point of the travelling wave vibrates at the equilibrium position, its vibration and energy spread along the direction of wave propagation, and the average energy density is not zero in one period. The travelling wave can be expressed as:

$$\xi(x, t) = A \cos \left(\omega t - \frac{2\pi}{\lambda} x \right) \quad (2)$$

Two standing waves which met some certain conditions can generate a travelling wave. Assume two standing waves (named as ξ_1 , ξ_2) have the same amplitude A , wave number k , angular frequency ω , and the same vibration direction, but $\pi/2$ difference in time and space respectively, then these two standing waves can be expressed as:

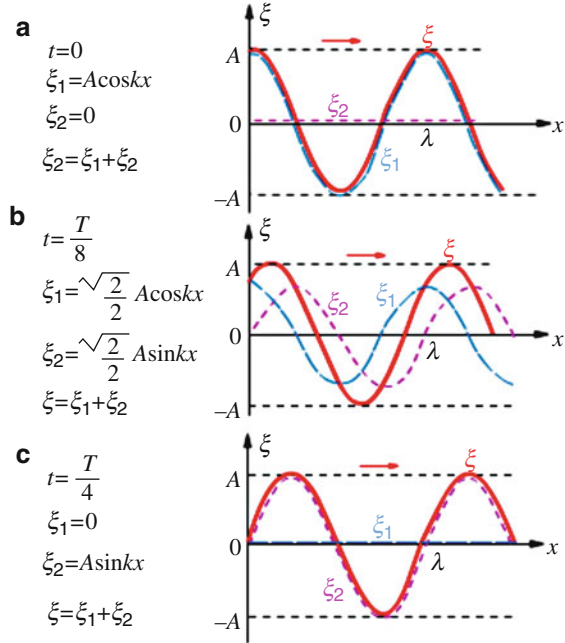
$$\begin{aligned} \xi_1(x, t) &= A \cos kx \cdot \cos \omega t = A \sin(kx + \pi/2) \sin(\omega t + \pi/2) \xi_2(x, t) \\ &= A \sin kx \cdot \sin \omega t \end{aligned} \quad (3)$$

Combining these two standing waves, a travelling wave ξ can be obtained:

$$\begin{aligned} \xi(x, t) &= \xi_1(x, t) + \xi_2(x, t) \\ &= A \cos kx \cdot \cos \omega t + A \sin kx \cdot \sin \omega t \\ &= A \cos(\omega t - kx) \end{aligned} \quad (4)$$

Thus, two standing waves with phase difference of $\pi/2$ could generate a travelling wave propagating along the positive direction of axis x , and the amplitude A , wave

Fig. 1 Waveform diagram of the superposition process of two standing waves



number k , and angular frequency ω of the travelling wave are same to the original standing waves. The superposition process of two standing waves at different time can be directly expressed by the waveform curve in Fig. 1.

According to the above expressions, when the following conditions (Eq. 5) are met, two wave standing wave will generate a travelling wave propagating along the positive direction of axis x .

$$(\varphi_2 + a_2) - (\varphi_1 + a_1) = \pm(2m + 1)\pi \quad (m = 0, 1, 2, \dots) \tag{5}$$

Similarly, four square standing waves with the same amplitude, frequency, direction of vibration, and phase difference of $\pi/2$ can be expressed as:

$$\begin{aligned} \xi_A(t) &= \frac{4h}{\pi} \left(\sin \frac{2\pi}{\lambda} x \sin \omega t + \frac{1}{3} \sin \frac{2\pi}{\lambda} 3x \sin 3\omega t + \dots \right) \\ \xi_B(t) &= \frac{4h}{\pi} \left(\cos \frac{2\pi}{\lambda} x \cos \omega t + \frac{1}{3} \cos \frac{2\pi}{\lambda} 3x \cos 3\omega t + \dots \right) \\ \xi_C(t) &= \frac{4h}{\pi} \left(\sin \frac{2\pi}{\lambda} x \sin \omega t + \frac{1}{3} \sin \frac{2\pi}{\lambda} 3x \sin 3\omega t + \dots \right) \\ \xi_D(t) &= \frac{4h}{\pi} \left(\cos \frac{2\pi}{\lambda} x \cos \omega t + \frac{1}{3} \cos \frac{2\pi}{\lambda} 3x \cos 3\omega t + \dots \right) \end{aligned} \tag{6}$$

The above four square standing waves can be combined into a square travelling waves.

$$\begin{aligned}
\xi(t) &= \xi_A(t) + \xi_B(t) + \xi_C(t) + \xi_D(t) \\
&= 2\frac{4h}{\pi} \left[\left(\sin \frac{2\pi}{\lambda}x \sin \omega t + \cos \frac{2\pi}{\lambda}x \cos \omega t \right) + \right. \\
&\quad \left. \frac{1}{3} \left(\sin \frac{2\pi}{\lambda}3x \sin 3\omega t + \cos \frac{2\pi}{\lambda}3x \cos 3\omega t \right) + \dots \right] \\
&= \frac{8h}{\pi} \left[\cos \left(\frac{2\pi}{\lambda}x - \omega t \right) + \frac{1}{3} \cos 3 \left(\frac{2\pi}{\lambda}x - \omega t \right) + \dots \right] \\
&= \frac{8h}{\pi} \left[\sin \left(\frac{\pi}{2} + \omega t - \frac{2\pi}{\lambda}x \right) + \frac{1}{3} \sin 3 \left(\frac{\pi}{2} + \omega t - \frac{2\pi}{\lambda}x \right) + \dots \right] \quad (7)
\end{aligned}$$

Thus, the four square standing waves which have difference of $\pi/2$ in time and space can also generate a square travelling wave; the travelling-wave micropumps are also based on this principle, generating the travelling wave in the elastic microchannels, and realizing the transport of the fluid.

The configuration parameters of the micropump are determined by the calculations and simulations below. The actuator array composes of four actuators, which have $1/4$ wavelength spacing between adjacent actuators. The voltage signals applied to the actuator array have the same amplitude, frequency, and different phase differed $\pi/2$ between the driving signals of adjacent actuator. The microchannel is made from PDMS (Sylgard 184, Dow Corning) which comprises the base and the curing agent with volume ratio of 10:1. In this condition, the Young's modulus of PDMS is $E \approx 750$ kPa, and the Poisson's ratio is $\nu \approx 0.45$ (Schwarz et al. 2002), and the shear modulus G is gained from the following equation:

$$G = E/2(1 + \nu) = 258.62\text{kPa} \quad (8)$$

Then, the velocity of transverse wave in the elastic channel is:

$$v = \sqrt{G/\rho} \quad (9)$$

The density of PDMS is about 1.03 g/cm³. As a result of calculating, the travelling wave velocity in the microchannel is $v = 15.8$ m/s, and the frequency of driving signals caused travelling wave propagating along positive x direction is about 1,886 Hz, as the spacing of piezoelectric actuators is 2.1 mm.

The average flow velocity is expressed by the following equation (Ogawa et al. 2009):

$$\bar{u} = \frac{1}{2}a^2\Psi(z) \quad (10)$$

Where a is the amplitude of the travelling wave, $\Psi(z)$ is a function of the microchannel's height. So the average flow velocity is proportional to the intensity of the oscillation which is defined as the square of the amplitude of the travelling wave, assumed the microchannel's height z is a constant.

The travelling wave in the microchannel is a forced resonance caused by the vibrations of the actuator array. In general, the response curve of the resonance is not exactly symmetric about the resonant frequency. But towards the low damping forced resonance, the intensity of oscillation with a driving frequency ω is approximated by the Lorentzian function, which is symmetric about the resonant frequency Ω . And the theoretical expression of the average flow velocity of the micropump could be expressed as follows. Γ is a parameter dependent on the damping of the oscillation, which specifies the full-width at half-maximum (FWHM). The parameter Γ is also a measure of the sharpness of the resonance, the smaller Γ value responds to the sharper resonant peak.

$$\bar{u} \propto a^2 = I(\omega) \propto \frac{2}{\pi} \cdot \frac{\Gamma}{4(\omega - \Omega)^2 + \Gamma^2} \quad (11)$$

When the vibration transferred to the PDMS, the amplitude gets smaller because of the absorption of elastic PDMS. Figure 2 shows the response of the maximum displacement of the microchannel's inside wall to the vibration amplitude on the microchannel's outside wall, which resulted from ANSYS. It is a conclusion that the curve is almost linear and the transfer efficiency of the amplitude is more than 93%.

The principle of the travelling-wave micropump is that the alternating voltage is transformed to the mechanical vibration by the actuator array, which induces a travelling wave on the elastic microchannel. The actuator array is attached to the surface of the microchannel, and the vibration of each actuator with different phase is transmitted to the corresponding position of the microchannel. The fluid particles beneath the top wall of the microchannel moves up-and-down followed the vibration of the top wall, and also moves forth and back due to the periodic variation of the local pressure in the microchannel, which caused by the travelling wave propagating along. Such two motions make the trajectory of fluid particles as an elliptic form. After a period of the travelling wave, the fluid particles move forward along the microchannel slightly. And the net flow at the outlet is achieved by repeating such motion.

Structure and Fabrication

Piezoelectric Travelling-Wave Micropump

The piezoelectric travelling-wave micropump mainly includes three parts: the micropump substrate, microchannel, and piezoelectric actuator array, shown in Fig. 3. The micropump substrate made from PMMA is used to support the microchannel and the piezoelectric actuator array, which consists of inlet, outlet, and actuator array slot (not illustrated in Fig. 3). The actuator array is attached on the microchannel and also connected to the voltage signals of different phase, which induces the travelling wave in the top wall of the microchannel.

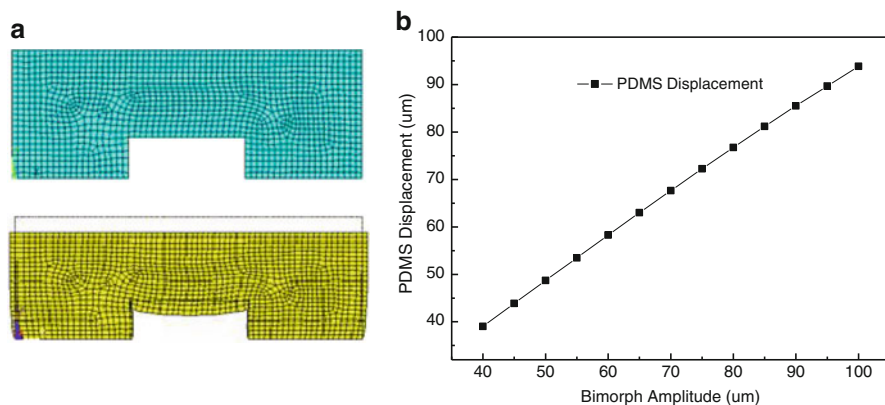


Fig. 2 Response of the maximum displacement of the microchannel to the vibration amplitude. (a) Simulation diagram of the microchannel with displacement of 0 and 50 μm ; (b) response curve of the maximum displacement of the microchannel's inside wall

The microchannel made by PDMS is an important part of travelling-wave micropump, as its elasticity and configuration affects the performance of the micropump directly. PDMS is a polymer material which exhibits very well optical transparency and biological inertia. It is also convenient to fabricating an integrated micropump by binding with silicon, glass, polystyrene, etc. The different microchannel structures of pump area are designed as the saw-tooth figuration and straight figuration, and the bumps on the top of the microchannel transferred the deformation caused by external pressures to the microchannel inside effectively. Figure 4 shows the configuration of saw-tooth channel. Because of the larger flank area and less pressure loss, the saw-tooth channel should exhibit less fluidic impedance than the straight channel and the traditional diffuse/nozzle structure.

The saw-tooth microchannel is a cascaded configuration of four diffuse elements; the parameter of each diffuse element is that the width of inlet is 200 μm , the width of outlet is 700 μm , the length of diffuse element is 2.1 mm, the height of microchannel is 100 μm , the thickness of side wall and top wall of the microchannel is 300 and 200 μm , and the height of the trapeziform bumps on the top wall is 100 μm .

The molds of microchannel are made from PMMA which has good chemical stability and mechanical performance. Firstly, the PDMS base and curing agent with volume ratio of 10:1 are mixed sufficiently. And the mixture is injected to the molds after degassing in the relative vacuum of -1 kg/cm^2 pressure. The molds are put into the incubator of 65 $^{\circ}\text{C}$ about 30 min, made the PDMS precuring. The microchannel which are shown in Fig. 4 are finished after stripping from the molds subsequently and put into a clean container and treated in UV of low pressure mercury lamp for 3 h.

Afterwards, the glass was treated to clean organic residues by piranha solution (98% H_2SO_4 :30% $\text{H}_2\text{O}_2 = 7:3$), rinsed extensively in distilled water for several times and dried thoroughly. Then the PDMS microchannel after UV treatment is put

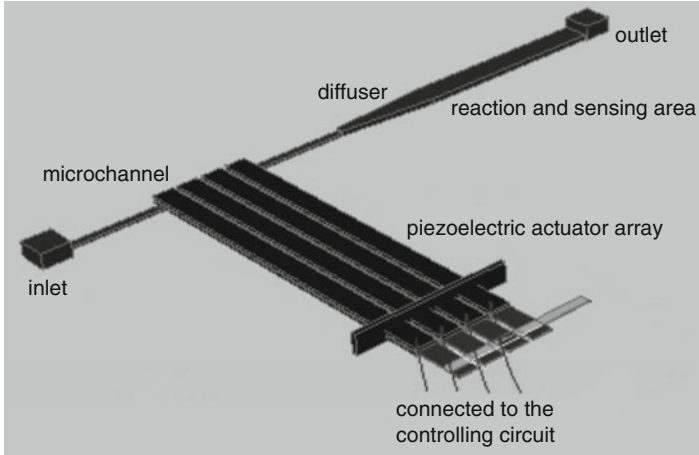


Fig. 3 Diagram of the travelling-wave micropump

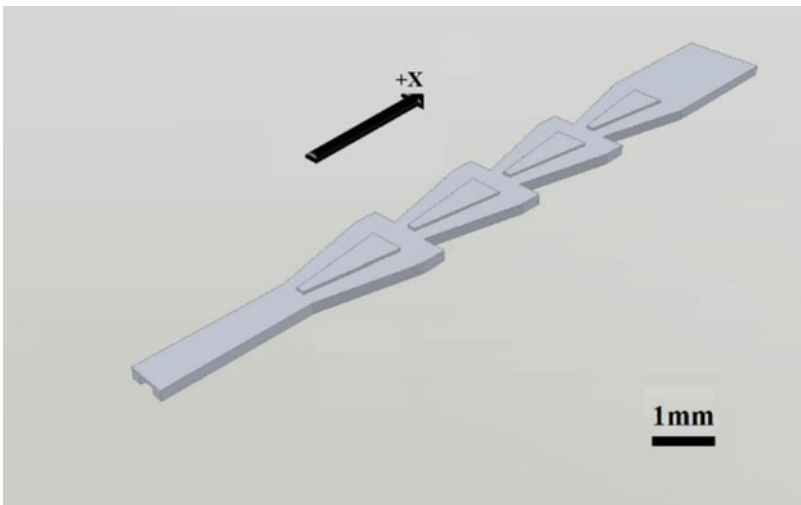
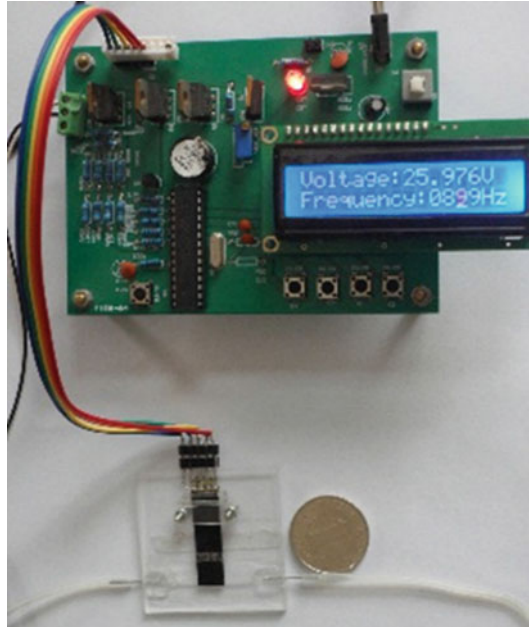


Fig. 4 Configuration of the saw-tooth microchannel

on the glass substrate and baked at 65 °C for 12 h to bonding the microchannel on the glass, while the additional pressure always lay on the microchannel. And the bonded PDMS microchannel fabricated by this method has enough watertight for the requirement of the travelling-wave micropump.

Finally, the piezoelectric actuator array is fixed on the pump area of microchannel, while the top of the cantilever is contacted on the bumps surface of microchannel. Four piezoelectric bimorphs of actuator array are parallel distributed

Fig. 5 Photograph of the piezoelectric travelling-wave micropump



with spacing of 2.1 mm. The photograph of the fabricated piezoelectric travelling-wave micropump is shown in Fig. 5.

Magnetic Travelling-Wave Micropump

The magnetic travelling-wave micropump employs two actuated micromagnet arrays and a saw-toothed microchannel to provide unidirectional fluid flow. Figure 6a shows an expanded diagram of the structure of the magnetic micropump. From bottom to top, it comprises three layers, namely a lower PMMA substrate containing an outlet and an inlet, a saw-toothed microchannel, and an upper PMMA substrate containing four round cavities. Specifically, the lower substrate was designed to combine with the microchannel, and the four round cavities in the upper substrate were molded and integrated with the cylindrical micromagnet array. A DC electric minimotor (6 mm in diameter and 14 mm in length) was mounted on the top side of the upper substrate. The gap between the ring-shaped magnets and the upper substrate is $d_1 = 0.8$ mm, and the interval between adjacent cylindrical magnets is $d_2 = 1$ mm.

Figure 6b presents the cross-sectional view of the magnetic micropump. The saw-toothed microchannel was bonded onto the lower substrate and covered by the upper substrate. For easy assembly, four cylindrical permanent micromagnets (each 2 mm in height and 1 mm in diameter, with $B = 500$ Gs at 1 mm above its surface) with the same magnetic pole orientation were embedded in the round

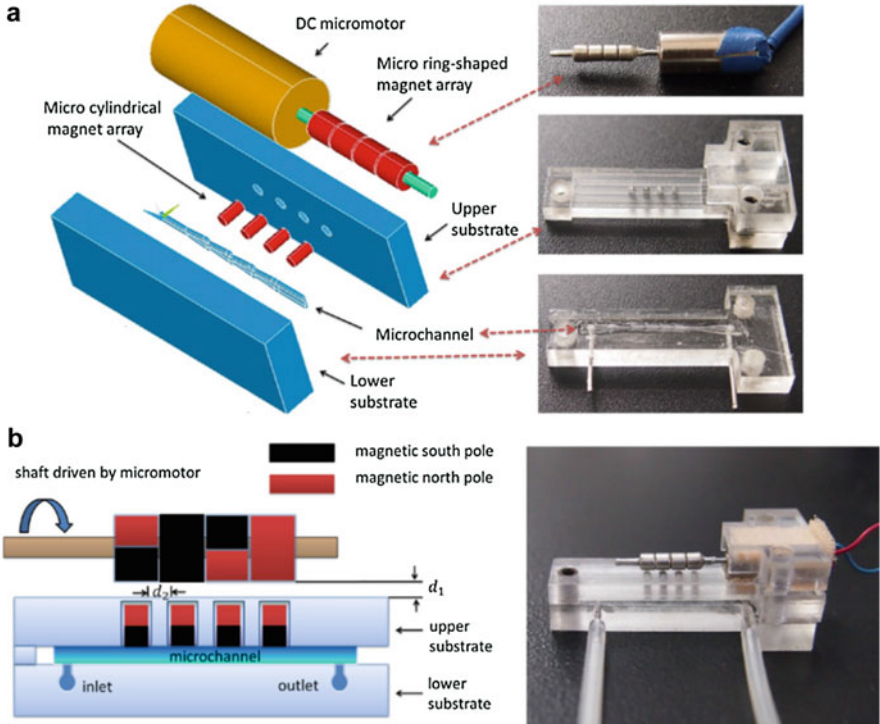


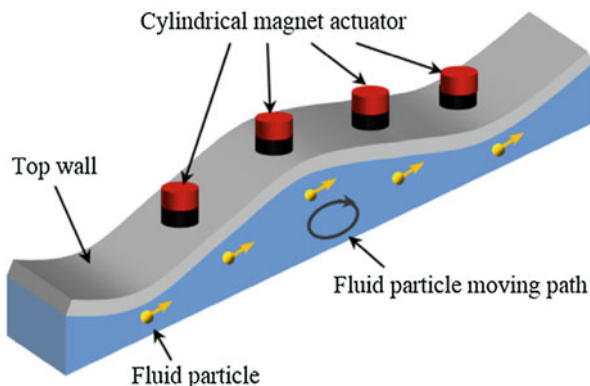
Fig. 6 Schematic of the magnetic travelling-wave micropump. (a) 3D components schematic; (b) cross-sectional view

cavities of the upper substrate side by side and in contact with the ceiling wall the elastic microchannel. Another four ring-shaped permanent micromagnets (each 2 mm in height, 1 mm in inner diameter, and 2.3 mm in outer diameter, with $B = 800$ Gs at 1 mm above its surface) were mounted on the rotation shaft of the motor and aligned to the cylindrical magnets one by one. The magnetic pole orientations of the ring-shaped magnets were arranged to successively rotate through $\pi/2$ rad. The gap between the ring-shaped magnets and the upper substrate is $d_1 = 0.8$ mm, and the interval between adjacent cylindrical magnets is $d_2 = 1$ mm. In this configuration, the travelling wave was induced beneath the ceiling wall by the rotating magnetic field created by these two magnetic arrays.

In Fig. 6, the cylindrical magnet actuators were arranged with the same magnetic pole orientation, and the ring-shaped magnets were arranged with the different magnetic pole orientation of rotating $\pi/2$ rad in turn. During one rotation cycle of the motor, the four cylindrical magnet actuators generate four standing waves with the same amplitude but with $\pi/2$ rad phase differences.

Therefore, the pumping mechanism is based on the successive actuation of the two micromagnet arrays, and the travelling wave is responsible for the fluid displacement

Fig. 7 Working mechanism of magnetic travelling-wave micropump



in the microchannel. Figure 7 shows the fluid particles beneath the top wall of the microchannel moving forward with the travelling wave due to its viscosity and the periodic variation of the local pressure. The flow rate of the liquid particles can be controlled by changing the frequency of the generated travelling wave.

The microchannel was fabricated by polydimethylsiloxane (PDMS) molding technology. First, the PDMS base and curing agent were mixed sufficiently with a volume ratio of 11:1. The mixture was injected into the PMMA molds after degassing in a relative vacuum of -1 kg cm^{-2} pressure and cured at $50 \text{ }^\circ\text{C}$ for about 50 min. Afterward, the microchannel was finished after stripping from the mold and treated by UV from a low-pressure mercury lamp for 3 h in a clean container. Then, the PDMS prepolymer was coated on the lower substrate and cured at $45 \text{ }^\circ\text{C}$ for about 30 min. Subsequently, the microchannel was bonding to lower substrate at $45 \text{ }^\circ\text{C}$ for 2 h. The bonded PDMS microchannel fabricated by this method is watertight enough for the requirements of the travelling-wave micropump. Finally, the cylindrical micromagnet array was embedded in the upper substrate, while the minimotor was mounted on the top side of the upper substrate. The upper and lower substrates were fixed by three bolts as shown in Fig. 6b.

The photograph of the micropump and drive circuitry is illustrated in Fig. 8. The motor was driven by programmable pulse-width-modulation (PWM) square waveforms ($V_{p-p} = 3.7 \text{ V}$), which were generated by an MSP430 microcontroller circuitry. Travelling waves with various frequencies ranging from 1 to 1.6 kHz were applied to the tested device, corresponding to motor rotation speeds from 15,000 to 24,000 rpm (approximately).

Performance

To optimizing the performance of the travelling-wave micropump, the piezoelectric travelling-wave micropump and magnetic travelling-wave micropump should be tested. The optimization of the travelling-wave micropump includes the

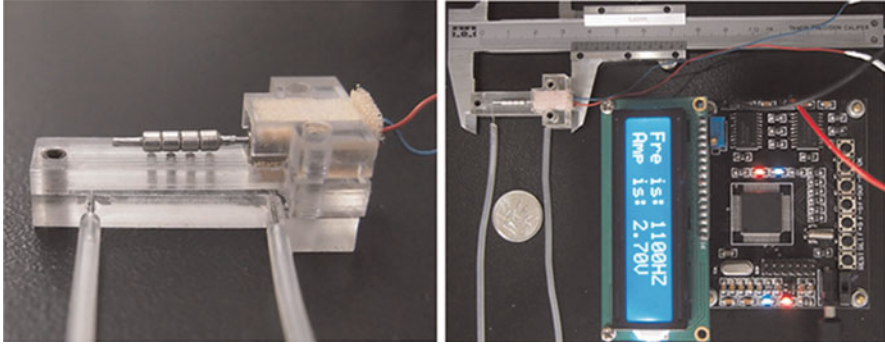


Fig. 8 Photograph of the micropump and drive circuitry

configuration, height of the microchannel, and the diffusion angle of the diffuser element. First, the piezoelectric travelling-wave micropumps with different microchannel are tested to compare the performance of different configuration of microchannels. And then, the performance of magnetic travelling-wave micropumps with different height and diffusion angle of saw-tooth microchannels are also tested, optimizing the parameters of microchannels.

Piezoelectric Travelling-Wave Micropump with Different Channels

The frequency property of two micropumps with different microchannel configuration is tested in the same conditions firstly. And then, at a certain frequency, the relationship of flow rate to back pressure and the voltage amplitude property are also tested. The back pressure is a pressure at the outlet caused by the output liquid of the micropump, which relates to the tightness, export capability of the pump, and the configuration of the channel. In the experiments, the adjustment of the back pressure is achieved by the height change of the liquid level at the micropump's outlet.

Figure 9 shows the dependency of average flow rate of micropumps with different microchannels on frequency when the voltage amplitude is fixed at 26 V. The average flow rate of micropump with the saw-tooth microchannel reaches the maximum of 33.36 $\mu\text{L}/\text{min}$ when the frequency of driving signal is 1,437 Hz, and that with the straight microchannel is only 24.88 $\mu\text{L}/\text{min}$ at the same frequency. At both sides of the maximum, the average flow rate is declined rapidly. The corresponding frequency of maximal flow rate in experiment (1437 Hz) is different to that in theory (1886 Hz), which is mainly caused by the error of the calculated elastic modulus of PDMS, but the calculated result is still a valuable reference.

The function fitting of the experimental data according to Eq. 4 is also shown in Fig. 9. The resonant central frequency Ω and the FWHM Γ of the fitting curve of the saw-tooth microchannel are 1439.7 and 374.4, respectively, and these two parameters of the straight microchannel are 1431.5 and 394.8, respectively. It is concluded

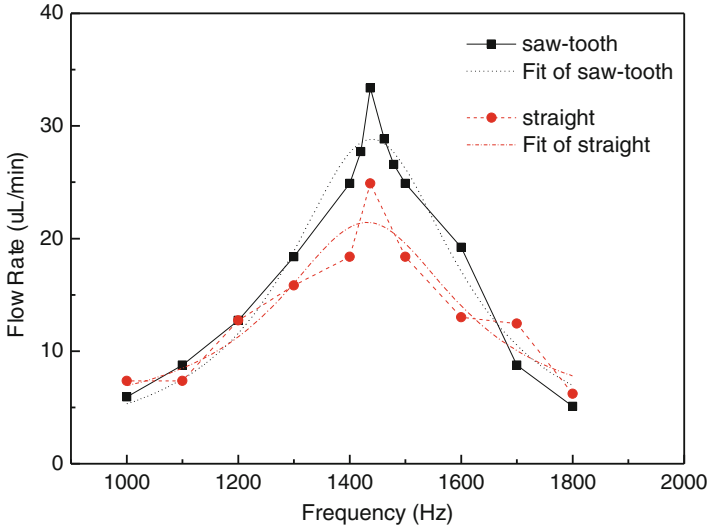


Fig. 9 Comparison between saw-tooth microchannel and straight microchannel

that the resonant frequencies of these two microchannels are basically the same, and the FWHM of the saw-tooth microchannel is smaller than that of the straight microchannel, indicating the better frequency selectivity.

From Fig. 9, it can be concluded that the saw-tooth microchannel can produce larger flow rate, and the frequency of maximum flow rate is the same for the two kinds of microchannels as the elastic modulus of the microchannel is unchanged. The same frequency of maximum flow rate infers that the frequency property is only dependent on the material property of the microchannels and independent on the structure.

Besides, the maximum back pressure of saw-tooth microchannel reaches 1.13 kPa, which is much larger than that of the straight microchannel (0.64 kPa). The curve of the flow rate to the back pressure is shown in Fig. 10. The curve shows the inverse proportion between average flow rate and back pressure of the micropump at driving frequency of 1,437 Hz. With the same flow rate, the micropump with saw-tooth microchannel could achieve larger back pressure than that with straight microchannel, because of the larger fluidic impedance along the reverse direction.

From Eq. 10, the average flow rate is proportional to the square of the voltage amplitude of driving signal. The voltage amplitude is picked as 20 V, 22 V, 24 V, 26 V, 28 V, respectively, and the average flow rate of the micropump is detected at frequency of 1,437 Hz. The fitting curve which is similar to the quadratic function and in accordance with the theoretical equation exactly is shown in Fig. 11.

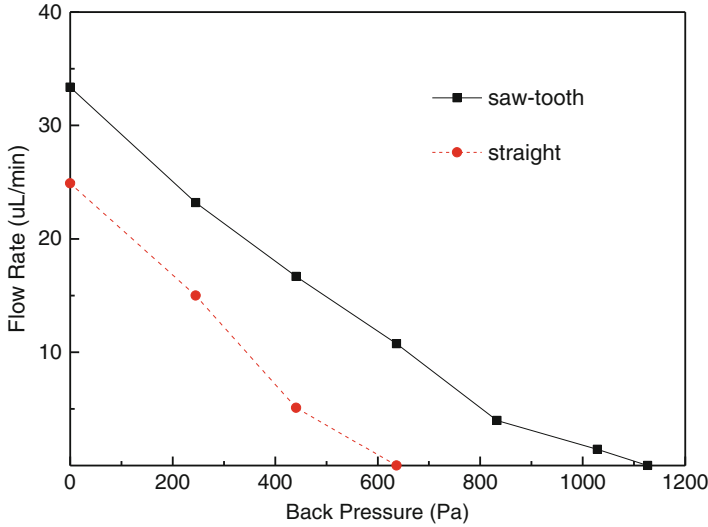


Fig. 10 Curve of flow rate to back pressure

Magnetic Travelling-Wave Micropump with Different Parameters

During testing, deionized water was used as a sample liquid for characterization of the micropump. Figure 12 shows the schematic of the micropump experimental setup and the averaged flow rate was tested (calculated by measuring the moving speed of the water front in the outlet tubing). In back pressure-related micropump tests, a pressure difference was obtained by placing the inlet and outlet tubes at a different height H and could be calculated as $\Delta\rho = \rho gH$, where ρ is the density of water (10^3 kg m^{-3}) and g is gravitational acceleration.

The valveless magnetic travelling-wave micropump’s characteristics by varying the driving frequency and microchannel geometry is studied systematically. Transient flow measurements on the different micropumps show that they all have flow-directing properties with the diverging-wall direction as the positive direction. First, the diffusion angle of the diffuser element is fixed at 6.5° and then studied the magnetic micropump characteristics by increasing heights of the microchannel to find the optimal height, which is $350 \mu\text{m}$. The frequency response of the average micropump flow rates at varied heights of the microchannel is shown in Fig. 13a. It can be seen that the tested average pumping flow rates show a consistent trend with the driving frequency. Specifically, the flow rate initially increases with the frequency until it reaches a peak value at a certain frequency. The average flow rates decline steadily on both sides of the maximum, in correspondence with the principle of the travelling-wave micropump, which implies that only a certain frequency of the driving signal, depending on the mechanical properties of the PDMS materials and

Fig. 11 Voltage amplitude property of travelling-wave micropump

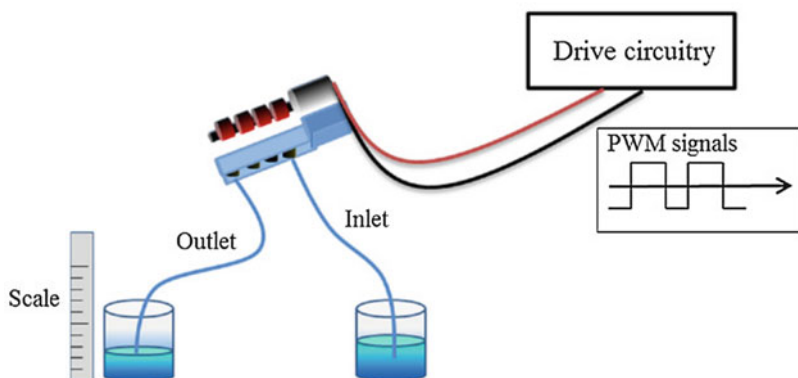
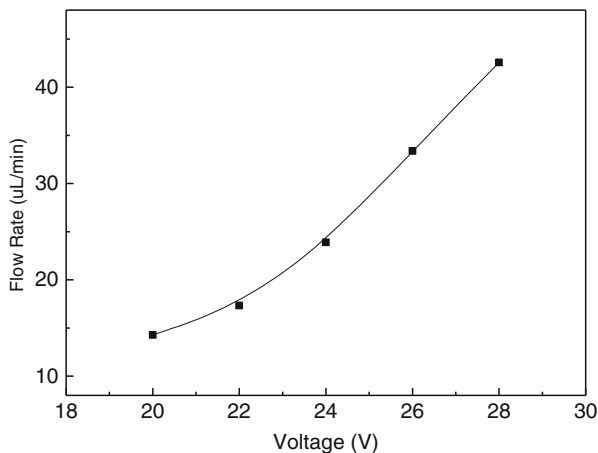


Fig. 12 Schematic of micropump experimental setup

the coupling between the channel and the flow, can efficiently induce a travelling wave in the microchannel.

Secondly, the height of the microchannel is fixed at $350\ \mu\text{m}$, and then the magnetic travelling-wave micropump characteristics is tested by increasing the diffusion angle of the diffuser element to find the optimal angle. Figure 13b clearly showed that average pumping flow rate increases with increasing diffusion angle of the diffuser element until it reaches an optimal angle of approximately 8° , which is in good agreement with previous studies. The behavior is proposed to be due to the flow separation as a result of the diffuser/nozzle elements, and further flow visualization investigation is required.

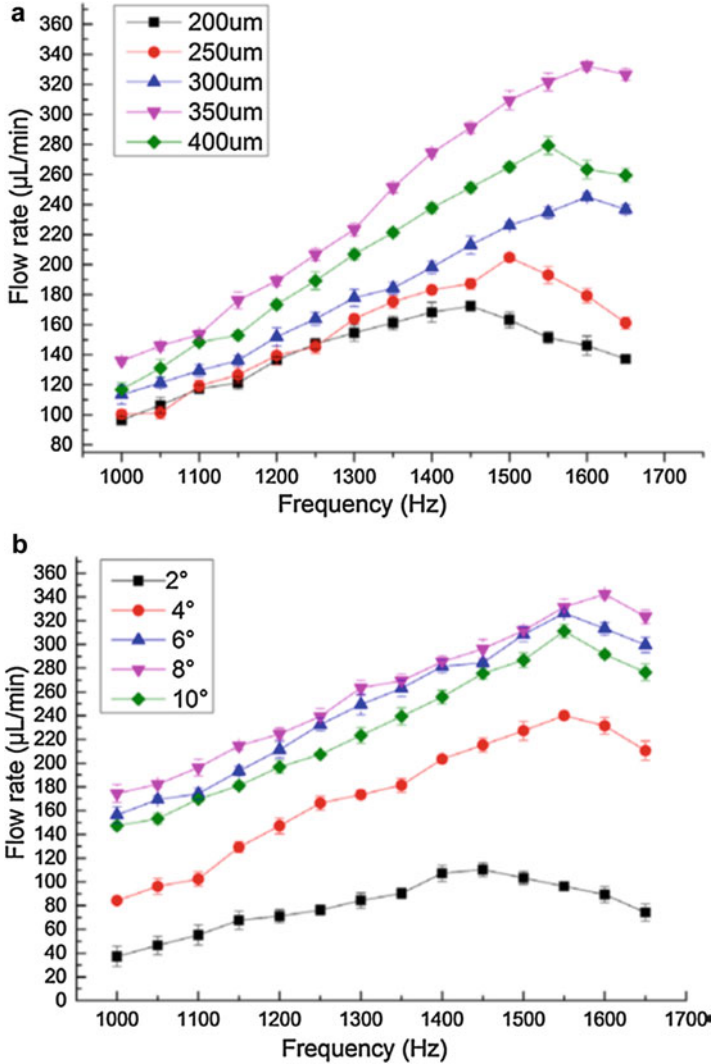


Fig. 13 Curve of average flow rates. (a) Flow rates at varied heights of the microchannel. (b) Flow rates at varied diffusion angles of the diffuser element

Figure 14a and b shows the relationship between the pumping flow rates and the back pressures at different driving frequencies. It can be observed that the pumping flow rates have an almost linear relationship with the back pressures. Accordingly, the magnetic micropump provides the maximum flow rate and back pressure ($342.4 \mu\text{L min}^{-1}$ and 1.67 kPa) with the height of the microchannel ($350 \mu\text{m}$) and the diffusion angle of the diffuser element (8°).

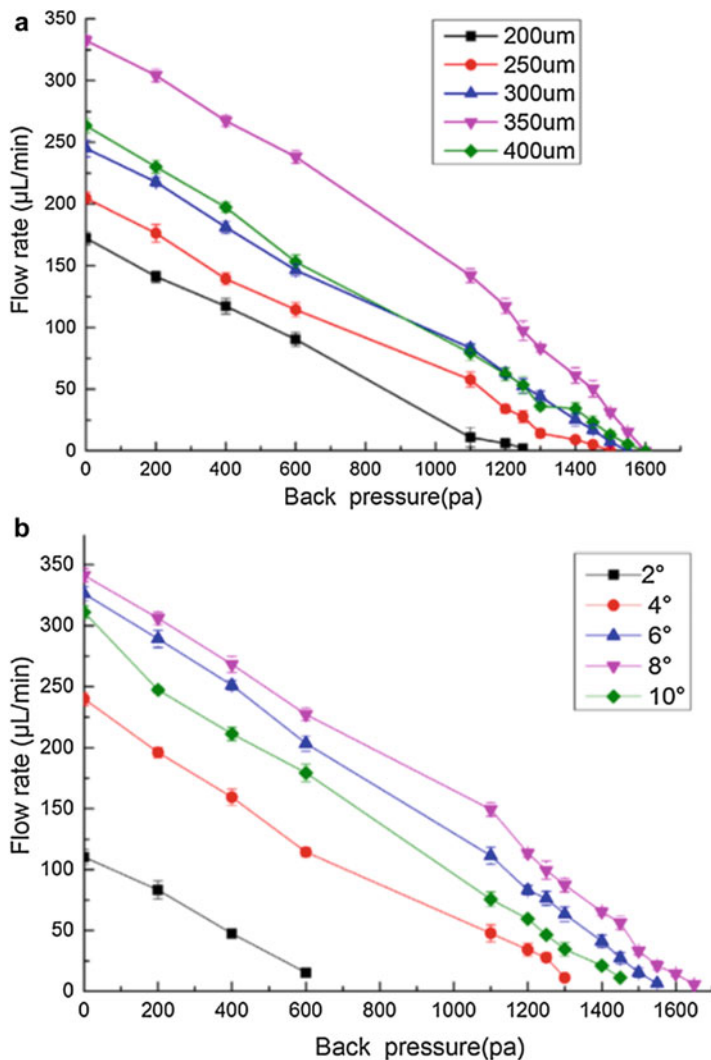


Fig. 14 Curve of flow rates against back pressures. (a) Relationship between flow rates and back pressures at varied heights of the microchannel. (b) Relationship between flow rates and back pressures at varied diffusion angles of the diffuser element

Conclusion

A piezoelectric travelling-wave micropump combined with the saw-tooth microchannel is presented, and compared the performance of this micropump with straight microchannel. The inducing mechanism of the travelling wave is discussed and simulated. The performance of the micropump such as average flow rate and back

pressure exhibits improvement in contrast to the straight microchannel micropump. And the micropump is applied in low voltage, which is benefit to the miniaturization and the integration.

An efficient valveless magnetic travelling-wave micropump is also presented here, which is actuated by the interactive forces between two integrated magnetic arrays. This results in a simple pump structure and permits easy system integration. With flow-rate regulation realized by the rotation speed of the motor, the device exhibits excellent performance, demonstrating its ability to drive fluid continuously and efficiently by inducing a travelling wave in the microchannel. This micropump was fabricated using simple molding technology and bonding techniques. In particular, the micropump device under varying microchannel parameters is characterized systematically, including the height of the microchannel and the diffusion angle. Experimental results demonstrate that this micropump is able to efficiently generate a maximum average flow rate of $342.4 \mu\text{L min}^{-1}$ and reliably operate against high back pressures up to 1.67 kPa. In addition, the performance of a magnetic micropump can even be further improved by optimizing the assembling technology. It is reasonable to expect that a magnetic micropump with this simple structure design and reliable operation can be readily integrated with various actuation methods and potentially applied in various lab-on-a-chip systems, such as drug delivery systems.

References

- Darabi J, Ohadi MM, DeVoe D (2001) An electrohydrodynamic polarization micropump for electronic cooling. *J Microelectromech Syst* 10:98–106
- Iverson BD, Garimella SV (2008) Recent advances in microscale pumping technologies: a review and evaluation. *Microfluid Nanofluid* 5:145–174
- Jang J, Lee SS (2000) Theoretical and experimental study of MHD (magnetohydrodynamic) micropump. *Sensors Actuators* 80:84–89
- Muralit P (2005) Piezoelectric micromachined ultrasonic transducers based on PZT thin films. *IEEE Trans Ultrason Ferroelectr Freq Control* 52:2276–2288
- Ogawa J, Kanno I, Kotera H et al (2009) Development of liquid pumping devices using vibrating microchannel walls. *Sensors Actuators* 152:211–218
- Olsson A, Stemme G, Stemme E (1996) Diffuser-element design investigation for valveless pumps. *Sensors Actuators* 57:137–143
- Olsson A, Enoksson P, Stemme G et al (1997) Micromachined flat-walled valveless diffuser pumps. *J Microelectromech Syst* 6:161–166
- Olsson A, Stemme G, Stemme E (2000) Numerical and experimental studies of flat-walled diffuser elements for valveless micropumps. *Sensors Actuators* 84:165–175
- Schwarz US, Balaban NQ, Rivelino D et al (2002) Calculation of forces at focal adhesions from elastic substrate data: the effect of localized force and the need for regularization. *Biophys J* 83:1380–1394
- Wang C, Zhang W, Liu RP et al (2013) Time-division self-referencing multichannel spectral SPR sensor without mechanical scanning. *Electron Lett* 49:493–495
- Ye WX, Zhang W, Wang C et al (2014) Travelling wave magnetic valveless micropump driven by rotating integrated magnetic arrays. *Micro Nano Lett* 9:232–234
- Zengerle R (1995) A bidirectional silicon micropump. *Sensors Actuators* 50:81–86
- Zhang W, Wang C, Yue Z et al (2011) Travelling-wave piezoelectric micropump with low resistance microchannel. *Electron Lett* 47:1065–1066